Carrier and Symbol Synchronisation for LoRa Receivers

Alexandre Marquet, Nicolas Montavont

Carrier and Symbol Synchronisation for LoRa Receivers

Alexandre Marquet
IMT Atlantique, IRISA, F-35576 Cesson Sévigné, France
alexandre.marquet@imt-atlantique.fr

Nicolas Montavont
IMT Atlantique, IRISA, F-35576 Cesson Sévigné, France
nicolas.montavont@imt-atlantique.fr

Abstract

LoRa is one of the most popular transmission scheme for the Internet of Things (IoT). It is used in many applications such as home automation, smart cities and smart agriculture. It provides low bitrate transmissions over long ranges, using unlicensed Industrial, Scientific and Medical (ISM) bands. Being a relatively new, and proprietary modulation, there are still challenges and improvements to be addressed and discovered. In this article, we cover estimation, tracking, and correction of slow varying timing and frequency offsets. Both timing and frequency offsets can arise, in particular, when oscillators, found in radios, are either of poor quality, or aged. The latter scenario is a serious concern for IoT, where devices are envisioned to stay in operation during decades without maintenance. The proposed estimators are based on symbol-by-symbol processing of the output of the demodulator. Tracking and correction are then performed by including these estimators in a tracking loop. Simulations show that the proposed closed-loop system can efficiently and jointly track timing and frequency offsets, even at low SNR.

1 Introduction

The Internet of Things (IoT) is a paradigm in which "things" (or objects), usually simple sensors or actuators, are deployed to help monitor and control complex systems. These objects are connected to a global network following the principles of the Internet, using open and standardized protocols. Typical applications for IoT are entertainment, home automation, smart cities and factory monitoring and control. For example, for smart buildings, objects can be used to perform metering (water, electricity, etc.), or light and temperature automatic control. In the Industry 4.0, the IoT can be used in closed-loop systems, in order to monitor and possibly control production chains.

IoT devices are usually constrained in terms of energy. This means that they cannot embed a lot of processing power, nor can they afford high-bitrate transmissions. They need energy efficient transmission schemes, which usually come with low spectral efficiency (hence, low bitrates), by virtue of the Shannon limit [6, chap. 4].

LoRa is one popular modulation for IoT devices, along with Sigfox and 3GPP NB-IoT. It is a long-range, low-power communication technology aimed at constrained devices. The LoRa transmission scheme uses Chirp-Spread Spectrum (CSS) modulation: an energy-efficient modulation, that performs well under channels suffering from Doppler shift and multipath propagation. This transmission scheme, as well as the performance and properties of CSS modulated signals have been studied in various articles [1, 3, 5, 7, 10], and the LoRa modulation itself is patented [8]. However, there are only few works that covers time/frequency synchronization and tracking for LoRa and, more generally, CSS modulations [2, 9].

IoT sensors and actuators are envisioned with a very long lifetime (decades, typically). These sensors may be deployed in locations that make them difficult to be accessed. As a result, hardware maintenance or other physical operations are challenging. In particular, regular tuning of oscillators may not be possible, impacting their precision and stability, and inducing both time and frequency jitters. At the demodulator level, this jitter translates to Sampling Frequency Offset (SFO), and Carrier Frequency Offset (CFO), which cause serious performance degradations on communication systems that use CSS modulations.

While initial estimations of SFO and CFO can be done using a preamble, tracking is also needed to compensate for oscillators fluctuations. Considering this issue, the main contributions of this article are:

- A theoretical model of the impact of fine timing and frequency offsets on CSS modulated signals.
- A symbol-by-symbol estimator for fine frequency offsets.
- A symbol-by-symbol estimator for fine timing offsets.
- A tracking loop, based on the proposed estimators, that uses only one non-coherent demodulator, and whose loop filters are simple accumulators.

Simulations show that the proposed closed-loop system can

efficiently track slowly drifting SFO and CFO. In terms of bit-error rate (BER), it is able to almost completely cancel the performance hit induced by slowly drifting SFO and CFO.

The remainder of this article is organized as follows. First, in section 2, we give an overview of the literature on LoRa analysis, and time/frequency offset impairments compensation. Then, section 3 describes a continuous-time CSS signal model, including timing and frequency offsets impairments. In section 4, a theoretical analysis of the impact of time and frequency offsets on CSS modulation performance is given. Next, section 5 presents the contributions of this article. Finally, section 6 analyses and evaluates the performance of the proposed tracking loop, by means of simulations.

2 Related Work

Because of the proprietary nature of LoRa, several reverse-engineering efforts have been conducted to understand and analyze its properties. Knight *et al.* [4] made the earliest attempt to implement and document a LoRa decoder, with partial success. Later on, Robyns *et al.* [7] gave a thorough description of LoRa modulation and demodulation chains, but described a highly sub-optimal CSS demodulator. More recently Marquet *et al.* [5] presented procedures to determine the key-parameters of the different algorithms of LoRa transmission chain (code generator matrix, whitening sequences, etc.), compared several demodulation strategies for CSS, and assessed LoRa performance under time and frequency selective channels.

Regarding the CSS modulation, described in the LoRa patent of Seller *et al.* [8], a continuous-time expression of CSS modulated signals was given by Goursaud *et al.* [3], and a discrete-time baseband complex equivalent was derived by Marquet *et al.* [5]. Theoretical performance over Additive White Gaussian Noise (AWGN) channel and Rayleigh fading channels were given by Elshabrawy *et al.* [1].

Interestingly, timing and carrier frequency offset estimations and compensations for CSS modulated signal received very few research interest. The patents of Tanaka *et al.* [9] and Seller *et al.* [8] describe procedures to estimate timing offset and CFO, based on the detection of a preamble. More recently Ghanaatian *et al.* [2] proposed a method to track and correct SFO. They also described a CFO estimator, but no associated tracking algorithm. Moreover, their article does not cover the association of their two estimators, which would allow joint SFO and CFO estimation, as required by practical systems.

3 System Model

We consider the baseband complex equivalent of the signal resulting from the transmission of the vector $\mathrm{c} = \{c_n\}_{n\in[0;K-1]}$ of $K \in \mathbb{N}^*$ symbols $c_n \in [0;M-1]$ ($M \in \mathbb{N}^*$), using a CSS modulation. Considering an occupied bandwidth of B Hz and a symbol time of T seconds, such a CSS signal is defined as [5]:

$$s(t) = \sum_{n=0}^{K-1} g_{c_n}(t-nT) \quad \forall t \in \mathbb{R}. \tag{1}$$

The pulse-shape $g_c(t) \in \mathbb{C}$ is defined as:

$$g_c(t) = \Pi_T(t) e^{j\pi\frac{B}{T}t^2}.e^{j2\pi\frac{c}{T}t}.e^{-j2\pi\lfloor\frac{B}{T}t+\frac{c}{T}\rceil t}, \tag{2}$$

with $\lfloor\cdot\rceil$ the rounding operator, and $\Pi_T(t) = 1$ if $t \in [0;T[$, and $\Pi_T(t) = 0$ otherwise. The waveform corresponding to $g_0(t)$ is called a linear chirp, and $g_c(t)$ is obtained by frequency-shifting $g_0(t)$ by c/B Hz, and wrapping the obtained shifted linear chirp between 0 and B Hz (see Fig. 1). One can show that, when $B.T = M$, then $\{g_c(t)\}_{c\in[0;M-1]}$ forms an orthogonal set [10]:

$$\int_{-\infty}^{+\infty} g_i^*(t)g_j(t)\mathrm{d}t = T\delta_{i-j} \quad \forall i,j \in \mathbb{Z}, \tag{3}$$

where $\delta_i = 1$ if $i = 0$, and $\delta_i = 0$ $\forall i \in \mathbb{Z}^*$. Also, because pulse-shapes only last T seconds, as enforced by the term $\Pi_T(t)$ in (2), orthogonality is also guaranteed between successive symbols:

$$\int_{-\infty}^{+\infty} g_i^*(t-nT)g_j(t-qT)\mathrm{d}t = T\delta_{i-j}\delta_{n-q} \quad \forall i,j,n,q \in \mathbb{Z}. \tag{4}$$

Conversely, the CSS modulation belongs to the family of orthogonal modulations (just like frequency-shift keying, and pulse-position modulation, for example).

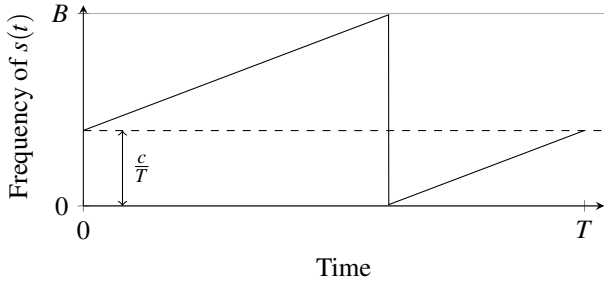

Figure 1. Frequency content of a chirp corresponding to the transmission of symbol $c = 50$, with $M = 128$.

A time and frequency shifted version of the signal (2) is received, corrupted by an Additive White Gaussian Noise $z(t)$:

$$r(t) = s(t-\delta t)e^{j2\pi\delta f t} + z(t), \tag{5}$$

with $\delta t \in \mathbb{R}$ (in seconds) and $\delta f \in \mathbb{R}$ (in Hz) the timing and frequency offsets, respectively.

Just like every other orthogonal modulation, its spectral efficiency is defined as [6, chap. 4]:

$$\eta = \log_2(M)/M. \tag{6}$$

This allows to define the per-bit signal to noise ratio as:

$$\frac{E_b}{N_0} = \frac{\log_2(M)}{M}\mathrm{SNR}, \tag{7}$$

where SNR is the signal-to-noise ratio.

4 Problem Statement

In this section, we analyze the impact of timing and frequency offsets on the transmission reliability. We consider a non-coherent receiver, which relaxes the need to estimate

phase-shifts impairments in the receiver. This means that each estimated symbol $\hat{c}_q$ is found by searching for the pulse-shape that correlate the best (in absolute value) with the received signal:

$$\hat{c}_q = \underset{\hat{c}\in[0;M-1]}{\operatorname{argmax}} \left| \int_{-\infty}^{+\infty} g_{\hat{c}}^*(t-qT) r(t) \mathrm{d}t \right| \tag{8}$$

$$= \underset{\hat{c}\in[0;M-1]}{\operatorname{argmax}} \left| \gamma_{q,\hat{c}} \right| \quad \forall q \in [0;K-1]. \tag{9}$$

In presence of timing (δt seconds) and frequency (δf Hz) offsets, we have:

$$\gamma_{q,\hat{c}} = \int_{-\infty}^{+\infty} g_{\hat{c}}^*(t-qT) s(t-\delta t) e^{j2\pi\delta f t} \mathrm{d}t + \underbrace{\int_{-\infty}^{+\infty} g_{\hat{c}}^*(t-qT) z(t) \mathrm{d}t}_{\text{Filtered noise term } z_{q,\hat{c}}.} \tag{10}$$

$$= \int_{-\infty}^{+\infty} e^{j2\pi\delta f t} \sum_{n=0}^{K-1} g_{\hat{c}}^*(t-qT) g_{c_n}(t-\delta t-nT) \mathrm{d}t + z_{q,\hat{c}}. \tag{11}$$

The summation in (11) includes a useful term (correlation with the portion of $r(t)$ carrying the q-th symbol), and an Inter-Symbol Interference (ISI) term (correlations with the portions of $r(t)$ carrying the symbols sent before or after the q-th one). We denote this term as: $\mathrm{ISI}_{q,\hat{c}} = \int_{-\infty}^{+\infty} e^{j2\pi\delta f t} \sum_{n\neq q} g_{\hat{c}}^*(t-qT) g_{c_n}(t-\delta t-nT)$. Using this notation, we obtain:

$$\gamma_{q,\hat{c}} = e^{j2\pi\delta f q T} \int_{-\infty}^{+\infty} e^{j2\pi\delta f t} g_{\hat{c}}^*(t) g_{c_q}(t-\delta t) \mathrm{d}t + \mathrm{ISI}_{q,\hat{c}} + z_{q,\hat{c}}. \tag{12}$$

In the ideal case, where $\delta t = 0$ and $\delta f = 0$, one can show that $\gamma_{q,\hat{c}} = T\delta_{\hat{c}-c_q} + z_{q,\hat{c}}\ \forall \hat{c} \in [0;M-1]$, by virtue of the orthogonality of the CSS modulation (4).

4.1 Fine Time and Frequency Offset

Let us focus on the value of γ_{q,c_q}, that is, assuming no demodulation error ($\hat{c} = c_q$). In this case, we have:

$$g_{c_q}^*(t) g_{c_q}(t-\delta t) = \Pi_T(t)\Pi_T(t-\delta t) e^{j\pi\frac{B}{T}\delta t^2} e^{-j2\pi\frac{B}{T}\delta t.t} e^{-j2\pi\frac{cq}{T}\delta t} e^{-j2\pi\lfloor \frac{B}{T}t+\frac{cq}{T}\rceil t} e^{j2\pi\lfloor \frac{B}{T}(t-\delta t)+\frac{cq}{T}\rceil (t-\delta t)}. \tag{13}$$

Assuming a fine timing offset ($\delta t \ll T$), we consider the following approximation:

$$g_{c_q}^*(t) g_{c_q}(t-\delta t) \approx \Pi_T(t) e^{j\pi\frac{B}{T}\delta t^2} e^{-j2\pi\frac{B}{T}\delta t.t} e^{-j2\pi\frac{cq}{T}\delta t}. \tag{14}$$

In the same spirit, we consider that the overlapping of adjacent symbols in time, due to timing offset, is negligible: $\mathrm{ISI}_{q,c_q} \approx 0$. Using these approximations, we get:

$$\gamma_{q,c_q} \approx e^{j2\pi\delta f q T} e^{j\pi\frac{B}{T}\delta t^2} e^{-j2\pi\frac{cq}{T}\delta t} \int_{-\infty}^{+\infty} \Pi_T(t) e^{j2\pi(\delta f - \frac{B}{T}\delta t).t} \mathrm{d}t + z_{q,c_q}. \tag{15}$$

Recalling that the inverse Fourier transform of $\Pi_T(t)$ is given as $\int_{-\infty}^{+\infty} \Pi_T(t) e^{j2\pi f t} \mathrm{d}t = T\mathrm{sinc}(\pi T f)$, we obtain:

$$\gamma_{q,c_q} \approx e^{j2\pi\delta f q T} e^{j\pi\frac{B}{T}\delta t^2} e^{-j2\pi\frac{cq}{T}\delta t} T\mathrm{sinc}(\pi(T\delta f - B\delta t)) + z_{q,c_q}. \tag{16}$$

On equation (16), we see that fine timing and frequency offsets lowers the noise sensibility, by lowering the power of the useful part of γ_{q,c_q}, with respect to noise (see Fig. 2). In particular, when $T\delta f - B\delta t = \Delta \in \mathbb{Z}^*$, then the useful part of γ_{q,c_q} completely vanishes. This case is analyzed in subsection 4.2.

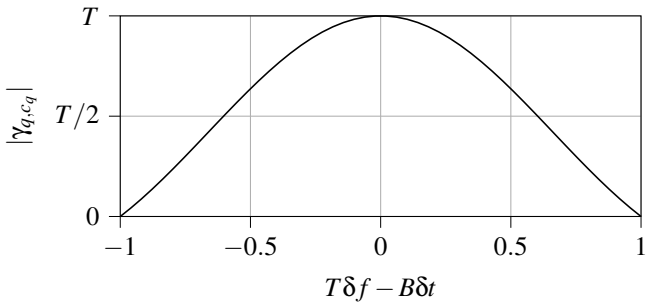

Figure 2. Impact of fine time and frequency offsets in absence of noise, on the magnitude of γ_{q,c_q}.

4.2 Coarse Time and Frequency Offset

Let us assume that $T\delta f - B\delta t = \Delta \in \mathbb{Z}^*$, and compute $\gamma_{q,\hat{c}}$ in this case. As in the previous subsection, we will assume that $\mathrm{ISI}_{q,\hat{c}} \approx 0$, which requires $\delta t \ll T$:

$$\gamma_{q,\hat{c}} \approx e^{j2\pi\delta f q T} \int_{-\infty}^{+\infty} e^{j2\pi\delta f t} g_{\hat{c}}^*(t) g_{c_q}(t-\delta t) \mathrm{d}t + z_{q,\hat{c}}. \tag{17}$$

As for the term under the integral, we use an approximation similar to (14):

$$g_{c_q}^*(t-\delta t) g_{\hat{c}}(t) \approx \Pi_T(t) e^{j\pi\frac{B}{T}\delta t^2} e^{j2\pi\frac{1}{T}(\hat{c}-c_q-\delta t.B)t} e^{-j2\pi\frac{\hat{c}}{T}\delta t}. \tag{18}$$

Combining the two last equations yields:

$$\gamma_{q,\hat{c}} \approx e^{j2\pi\delta f q T} e^{j\pi\frac{B}{T}\delta t^2} e^{-j2\pi\frac{\hat{c}}{T}\delta t} T\mathrm{sinc}(\pi(\Delta + \hat{c} - c_q)) + z_{q,\hat{c}}. \tag{19}$$

Because $\mathrm{sinc}(\pi n) = 1$ if $n = 0$ and $\mathrm{sinc}(\pi n) = 0\ \forall n \in \mathbb{Z}^*$ then, even in complete absence of noise ($z_{q,\hat{c}} = 0$), we have:

$$\hat{c}_q = \underset{\hat{c}\in[0;M-1]}{\operatorname{argmax}} \left| \gamma_{q,\hat{c}} \right| = c_q + \Delta \mod M. \tag{20}$$

To sum up, coarse timing or frequency offsets cause a constant error floor, even in the absence of noise.

More generally, any combination of timing and frequency offsets for which it exists $\Delta \in [0;M-1]$ such that $\mathrm{sinc}(T\delta f -$

$B\delta t) < \mathrm{sinc}(T\delta f - B\delta t \pm \Delta)$ induces an error floor. Motivated by this result, we formally define fine and coarse timing and frequency offsets as follows:

- Fine frequency offset: $|\delta f| < 0.5/T$.
- Fine timing offset: $|\delta t| < 0.5/B$.
- Coarse frequency offset: $|\delta f| \geq 0.5/T$.
- Coarse timing offset: $|\delta t| \geq 0.5/B$.

On the one hand, with these definitions, a fine timing (respectively, frequency) offset alone cannot yield an error floor. On the other hand, a coarse timing or frequency offset alone will systematically yield an error floor. Combinations of time and frequency offsets yields more complicated scenarii as, depending on their sign, they may either add up, or compensate each other in $T\delta f - B\delta t$.

5 Fine Time-Fequency Shift Estimation and Tracking

5.1 Fine Frequency Offset Estimation

In the following, we propose a frequency offset estimator that is robust against timing offsets. It basically consists in an estimation of the remaining phase variation between successive decision variables ($\gamma_{q,\hat{c}_q}$) using a quadrature detector. Let us assume perfect decisions ($\hat{c}_q = c_q \ \forall q \in [0;K-1]$), then:

$$\begin{aligned}\gamma_{q,\hat{c}_q}\cdot\gamma^*_{q-1,\hat{c}_{q-1}} \approx T\,\mathrm{sinc}(2\pi(T\delta f - B\delta t))\\ \Big[e^{j2\pi\delta fT}e^{-j2\pi\frac{\hat{c}_q-\hat{c}_{q-1}}{T}\delta t}T\,\mathrm{sinc}(2\pi(T\delta f - B\delta t))\\ + z^*_{q-1,\hat{c}_{q-1}}e^{j2\pi\delta fqT}e^{j\pi\frac{B}{T}\delta t^2}e^{j2\pi\frac{c_q}{T}\delta t}\\ + z_{q,\hat{c}_q}e^{-j2\pi\delta f(q-1)T}e^{-j\pi\frac{B}{T}\delta t^2}e^{-j2\pi\frac{c_{q-1}}{T}\delta t}\Big]\\ + z_{q,\hat{c}_q}z^*_{q-1,\hat{c}_{q-1}}. \quad (21)\end{aligned}$$

Assuming that symbols are Independent and Identically Distributed (IID), that noise samples are mutually independent, and independent from the modulated symbols, we have:

$$\mathbb{E}\{\gamma_{q,\hat{c}_q}\cdot\gamma^*_{q-1,\hat{c}_{q-1}}\} \approx e^{j2\pi\delta fT}T^2\mathrm{sinc}(2\pi(T\delta f - B\delta t))^2. \quad (22)$$

Motivated by this result, we propose to estimate δf as:

$$\hat{\delta f} \approx \frac{T}{2\pi}\arg\mathbb{E}\{\gamma_{q,\hat{c}_q}\cdot\gamma^*_{q-1,\hat{c}_{q-1}}\}, \quad (23)$$

where the expected value can by practically estimated by averaging successive values of $\gamma_{q,\hat{c}_q}\cdot\gamma^*_{q-1,\hat{c}_{q-1}}$.

One can notice that the frequency offset estimation of (23) is not susceptible to timing offsets, and is linear with δf. In practice, timing offset reduces the range of the estimator, as shown in the simulation of Fig. 3.

5.2 Fine Time Shift Estimation

In this subsection, we propose a timing offset estimator. Assuming perfect decisions ($\hat{c}_q = c_q$), it is straightforward for a receiver to generate any time-shifted version of $g_{c_q}(t - qT)$. Hence, the value of the time-shift could be recovered

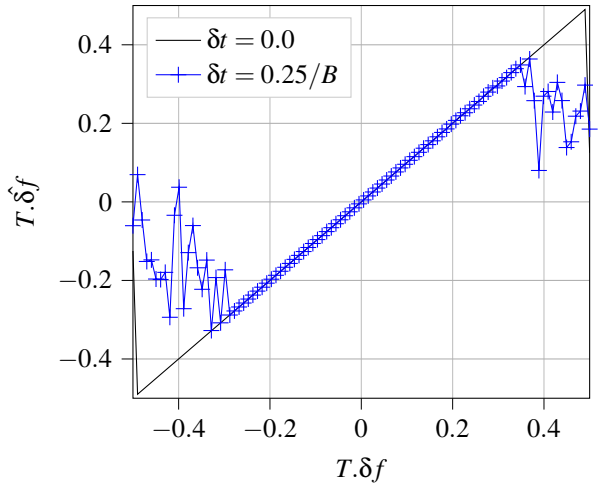

Figure 3. Simulation of the frequency offset estimator with $M = 512$ and no noise. We observe how a timing offset reduces the range of this estimator.

by finding the timing offset $\hat{\delta t}$ that allows the pulse-shape to correlates the best with the received signal:

$$\hat{\delta t} = \underset{\hat{\delta t}\in[-0.5/B;0.5/B[}{\mathrm{argmax}} \left|\int_{-\infty}^{+\infty} g^*_{\hat{c}_q}(t - qT - \hat{\delta t})r(t)\mathrm{d}t\right|. \quad (24)$$

However, because δt is a continuous quantity, it is not possible to evaluate (24) directly. One simple way to circumvent this limitation, is to discretize the search space with $N \in \mathbb{N}^*$ values:

$$\begin{aligned}\hat{\delta t} = -\frac{1}{2}\\ + \frac{1}{N}\underset{n\in[0;N-1]}{\mathrm{argmax}}\left|\int_{-\infty}^{+\infty} g^*_{\hat{c}_q}(t - qT - (n/N - 0.5))r(t)\mathrm{d}t\right|.\end{aligned} \quad (25)$$

Because of the discretization, the estimator (25) is piecewise constant linear with respect to δt (see Fig. 4). Interestingly, in practice, this estimator is not particularly susceptible to fine frequency offsets, as shown in simulations of Fig. 5.

5.3 Joint Time-Frequency Shift Correction

The frequency and timing offset estimators proposed in subsections 5.1 and 5.2, respectively, both require outputs from a non-coherent demodulator. Hence, the only solution, in order to use these estimators without requiring multiple demodulators, is to use feedback loops. This not only reduces the overall complexity of the receiver, but also allows to correct coarse time and frequency offsets ($|\delta t| > 1/B$ and $|\delta f| > 1/T$), as long as they result from slow variations (that is, fine timing and frequency offsets between successive symbols).

The proposed closed-loop system (see Fig. 6) is actually composed of two nested loops: one for the frequency offset compensation, and the other for the timing offset compensation. Both use a first-order IIR (Infinite Impulse Response)

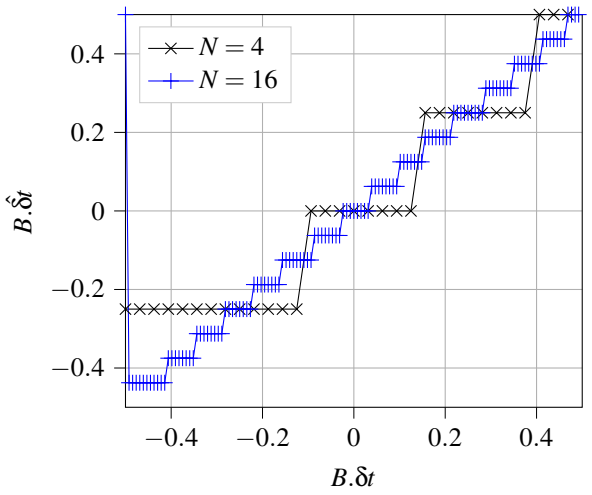

Figure 4. Simulation of the timing offset estimator with $M = 512$, no noise and various levels of discretization (N).

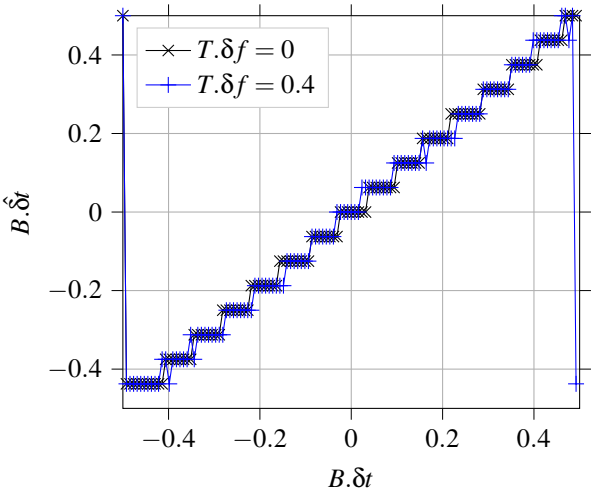

Figure 5. Robustness of the timing offset estimator to frequency offsets, with $M = 512$ and no noise.

loop filter, whose impulse response is given by:

$$H(z) = \frac{a}{1 - z^{-1}}, \tag{26}$$

where $a \in \mathbb{R}^{+*}$ is the gain of the loop. We denote a_f the gain of the frequency offset compensation loop, and a_t the gain of the timing offset compensation loop. Usually, to keep the loop stable, these gains are kept bellow unity: $a_t < 1$ and $a_f < 1$. This type of filters allow for very low-complexity updates of the estimates:

$$\hat{\delta t}_{q+1} = \hat{\delta t}_q + a_t \hat{\delta t} \quad \text{and} \quad \hat{\delta f}_{q+1} = \hat{\delta f}_q + a_f \hat{\delta f}, \tag{27}$$

where $\hat{\delta t}_q$ (respectively, $\hat{\delta f}_q$) is the filtered time (respectively, frequency) estimate after reception of the q-th symbol, and $\hat{\delta t}$ (respectively, $\hat{\delta f}$) is the output of the estimator, as given by (25) (respectively, (23)). Note that in this system, it is the loop filter that is in charge of approximating the expectancy in (23), by averaging successive values of $\gamma_{q,\hat{c}_q} \cdot \gamma^*_{q-1,\hat{c}_{q-1}}$. These filtered time and frequency offsets estimates are then used to drive a variable delay line and a Voltage Controlled Oscillator (VCO), in order to present the demodulator with a time and frequency synchronized signal.

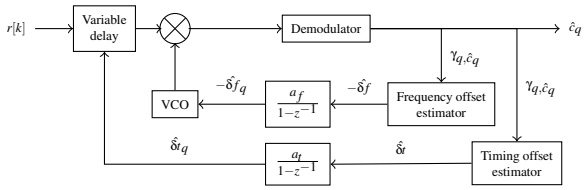

Figure 6. Timing and frequency offsets tracking using a loop and first order filters.

5.4 Discussion

The proposed timing and frequency offsets estimators, and the associated closed-loop system allows for low-complexity time-frequency synchronization under the hypothesis of an AWGN channel, and slow varying timing and frequency offsets.

It is worthwhile mentioning that both estimators, and the tracking loop, trade reactivity with complexity. Indeed, both estimators work on demodulated symbols, making them powerless in face of timing and frequency offsets that vary significantly during one symbol duration (T). In the same spirit, it might be interesting to study the relevance of higher order loop filter, that may enable better tracking of sudden timing and/or frequency offsets variations.

Also, the proposed frequency offset estimator is sensitive to any symbol-to-symbol phase variation, including random variations that may not be due to CFO. This means that, in practical system, a prior step of phase shift estimation and tracking might be needed.

6 Performance Evaluation

This section is dedicated to the analysis, by means of simulations, of the timing and frequency offset estimators proposed in section 5, as well as the tracking loop of Fig. 6.

On Fig. 7, one can observe the reactivity and stability of the loop when presented to a simultaneous change of timing

and frequency offsets, for various values of the loop gains a_t and a_f. For both loops, a gain between 0.3 and 0.4 gives a good compromise between loop reactivity and loop stability.

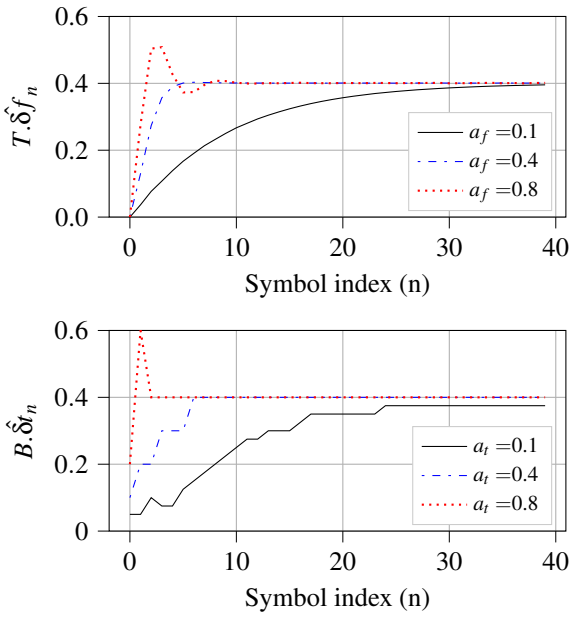

Figure 7. Response of the tracking loop to a simultaneous timing offset of $B.\delta t = 0.4$, and frequency offset $T.\delta f = 0.4$, with $M = 512$ and no noise. The timing offset estimator is set with $N = 4$.

Finally, Fig. 8 shows the behaviour of the closed-loop system in terms of Bit Error Rate (BER) when faced with slowly changing timing and frequency offsets. The time drifting is implemented with a sampling frequency offset. That means that the receiver uses a reference symbol time which is slightly different than T. This can be modelled as constant increase (or decrease) of the timing offset between successive symbols and, consequently, can be corrected by the tracking loop.

In this scenario, even though the consecutive symbols only experience fine timing and frequency offsets, the accumulating error can reach timing offsets such that $|\delta t| > 0.5/B$ and frequency offsets with $|\delta f| > 0.5/T$. We observe that the closed-loop system allows to recover performance very close to CSS over perfect AWGN channel (without timing and frequency offsets) with a penalty of around 0.4 dB of E_b/N_0.

7 Conclusion

In this article, we first gave a theoretical analysis of the implications of timing and frequency offsets on performance of CSS transmissions. Considering some approximations, this analysis shows that these two kinds of impairments yields to the same type of performance hits. Indeed, fine time and frequency offsets make the modulated signal more susceptible to noise, while coarse offsets lead to a constant symbol error floor.

Based on the analysis mentioned above, we derived a timing offset estimator, and a frequency offset estimator. The former proves to be resilient to frequency offsets, while the latter has is detection ranged reduced by timing offsets. By introducing this estimator in a simple closed-loop system, including the demodulator and an accumulator as loop filter, proved to be an effective solution for joint demodulation, timing and frequency offset tracking.

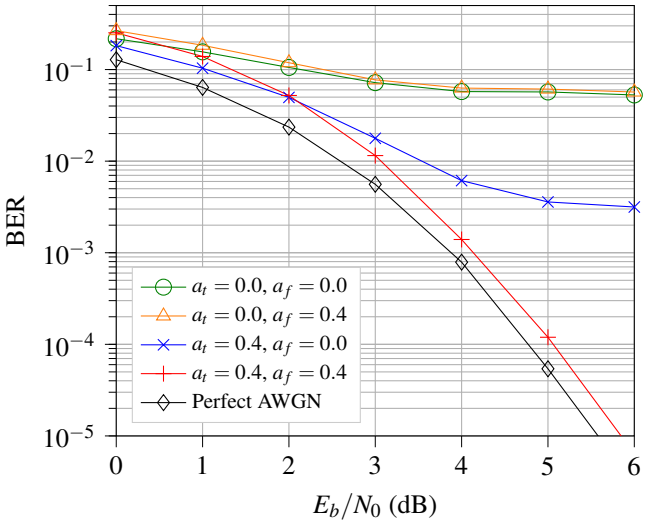

Figure 8. BER performance of the tracking loop of Fig. 6, with $M = 512$ and under Gaussian random walk sampling frequency and carrier frequency offset models. Both models have a standard deviation of 10^{-6}, and the maximum sampling frequency offset is set to 50 ppm (no limit for the carrier frequency offset). The timing offset estimator is set with $N = 4$.

8 References

[1] T. Elshabrawy and J. Robert. Closed-Form Approximation of LoRa Modulation BER Performance. *IEEE Communications Letters*, 22(9):1778–1781, Sep. 2018.

[2] R. Ghanaatian, O. Afisiadis, M. Cotting, and A. Burg. Lora digital receiver analysis and implementation. In *ICASSP 2019 - 2019 IEEE International Conference on Acoustics, Speech and Signal Processing (ICASSP)*, pages 1498–1502, May 2019.

[3] C. Goursaud and J.-M. Gorce. Dedicated networks for IoT : PHY / MAC state of the art and challenges. *EAI endorsed transactions on Internet of Things*, Oct. 2015.

[4] M. Knight and B. Seeber. Decoding LoRa: Realizing a Modern LPWAN with SDR. *Proceedings of the GNU Radio Conference*, 1(1), 2016.

[5] A. Marquet, N. Montavont, and G. Z. Papadopoulos. Investigating theoretical performance and demodulation techniques for lora. In *2019 IEEE 20th International Symposium on "A World of Wireless, Mobile and Multimedia Networks" (WoWMoM)*, pages 1–6, June 2019.

[6] J. Proakis and M. Salehi. *Digital Communications*. McGraw-Hill International Edition. McGraw-Hill, 2008.

[7] P. Robyns, P. Quax, W. Lamotte, and W. Thenaers. A Multi-Channel Software Decoder for the LoRa Modulation Scheme. In *Proceedings of the 3rd International Conference on Internet of Things, Big Data and Security - Volume 1: IoTBDS,*, pages 41–51. INSTICC, SciTePress, 2018.

[8] O. Seller and N. Sornin. Low power long range transmitter, 2014.

[9] H. Tanaka. A frequency and timing synchronization circuit making use of a chirp signal, 1999.

[10] L. Vangelista. Frequency Shift Chirp Modulation: The LoRa Modulation. *IEEE Signal Processing Letters*, 24(12):1818–1821, Dec 2017.